A New Optical Technique to Study Aerosol Phase Transitions: The Nucleation of Ice from H_2SO_4 Aerosols

Thomas Koop, Huey P. Ng, Luisa T. Molina, and Mario J. Molina*

Department of Chemistry and Department of Earth, Atmospheric, and Planetary Sciences, Massachusetts Institute of Technology, Cambridge, Massachusetts 02139

Received: June 30, 1998; In Final Form: September 2, 1998

A new optical microscope technique has been developed to investigate phase transitions in micrometer-sized droplets. This technique has been used to study the nucleation of ice from aqueous H_2SO_4 aerosols 0−35 wt % in composition in the temperature range from 273 to 170 K. The aerosols were produced with a nebulizer and were deposited on a quartz plate, which was coated with a hydrophobic silane monolayer to minimize the effects of heterogeneous nucleation. More than 1200 aerosol particles were monitored individually with the optical microscope, and their freezing temperatures and melting points were recorded. The observed freezing temperatures are lower than the ones from comparable aerosol studies reported in the literature, the differences in the freezing temperature being up to 30 K, especially for the more concentrated aerosols. No freezing was observed above 170 K for compositions greater than 27 wt %. A thermodynamic model has been used to apply the new freezing temperature data to the formation of clouds in the upper troposphere and lower stratosphere. The results indicate that the homogeneous nucleation of ice particles in cirrus clouds requires saturation ratios with respect to ice ranging from about 1.5 at 230 K to 1.6 at 205 K. In addition, the formation of type II polar stratospheric clouds under volcanically perturbed conditions where H_2SO_4 is the main aqueous aerosol component at low temperatures is predicted to occur about 3 K below the ice frost point.

Introduction

Clouds play an important role in the Earth's atmosphere. They strongly affect both the chemistry and radiative properties of the Earth. One of the biggest uncertainties in assessing the global radiation budget is the scattering of both incoming sunlight and infrared radiation from the Earth's surface by aerosols and cloud particles.[1] This uncertainty is mainly a consequence of the fact that the mechanisms involving the effects of aerosols on the formation of different types of clouds are still poorly understood.[1,2] Cirrus clouds cover up to about 20−30% of the Earth and, thus, play a large role in determining Earth's albedo.[3] Cirrus clouds are also important in the chemistry of the upper troposphere, where they provide surfaces for important heterogeneous reactions. Modeling studies have shown the potential for chlorine activation on cirrus-cloud particles and subsequent ozone destruction,[4] and field measurements indeed showed disturbed ozone concentrations in the presence of upper tropospheric clouds.[5,6] Finally, a detailed microphysical understanding of the formation of cirrus clouds is needed to assess the effect of aircrafts and contrails on the chemistry and the cloud coverage of the upper troposphere.[2,7] The general importance of polar stratospheric clouds (PSCs) in ozone chemistry of the polar regions is well understood.[8] Although a complex picture of how PSCs form has evolved over the past decade,[9] the details of some of the formation mechanisms remain poorly understood. However, a detailed knowledge of PSC microphysics might be of crucial importance to assess the possibility of very significant ozone depletion in the Arctic, especially in light of recent modeling studies suggesting major stratospheric cooling resulting from changes in global circulation patterns induced by rising greenhouse-gas concentrations.[10] Aqueous H_2SO_4 aerosols are ubiquitous in the upper troposphere and lower stratosphere and are involved in both the formation of cirrus clouds and PSCs. In this paper, we present new data on the nucleation of ice from H_2SO_4/H_2O aerosols and discuss the implications for cloud formation. Low-temperature studies on phase transitions in aerosol particles are usually performed in flow-tube or settling-chamber experiments.[11−15] The aerosol composition and the freezing is detected by means of Fourier transform infrared (FTIR) spectroscopy, i.e., by observing characteristic liquid H_2SO_4 and ice absorption features in the spectra, often relying on extrapolations from high-temperature calibrations to deduce aerosol compositions. The only published experimental study investigating the nucleation of ice from H_2SO_4/H_2O aerosols employs the flow-tube approach.[12] Recently, we have developed several new techniques to investigate the phase transitions of micrometer-sized particles (see e.g., Molina et al.[16]). The first technique involves differential scanning calorimetry of emulsions.[17] The second technique involves the use of infrared spectroscopy to monitor the phase transitions of particles attached to the inside surface of a gold-plated tube.[18] The third method, in which aerosol particles are deposited on an inert surface and then observed with an optical microscope while cooling, is presented here. Preliminary work involving the development of this new technique has been described by Ng.[19] This new technique enables a direct measurement of the composition and the freezing temperatures of the aerosols.

Experimental Section

General Description. The experimental apparatus and the sample cell are shown schematically in Figures 1 and 2, respectively. The setup consists of a Zeiss Axioskop 20 optical microscope equipped with a Linkam BCS 196 biological cold

* To whom correspondence should be addressed.

10.1021/jp9828078 CCC: $15.00
Published on Web 10/21/1998

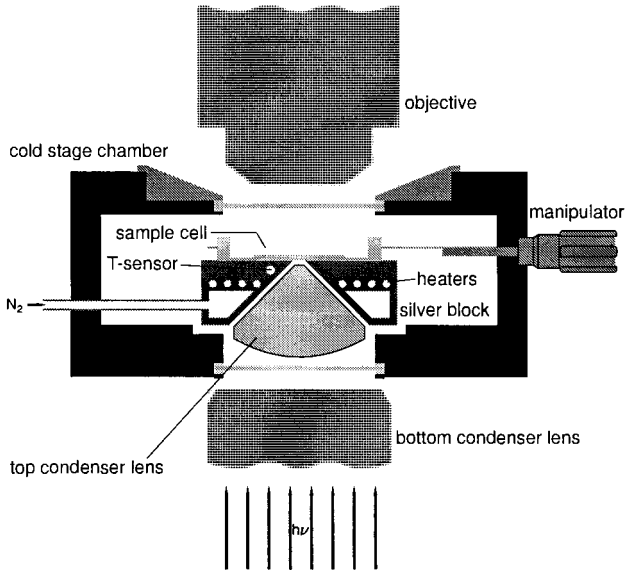

Figure 1. Experimental setup.

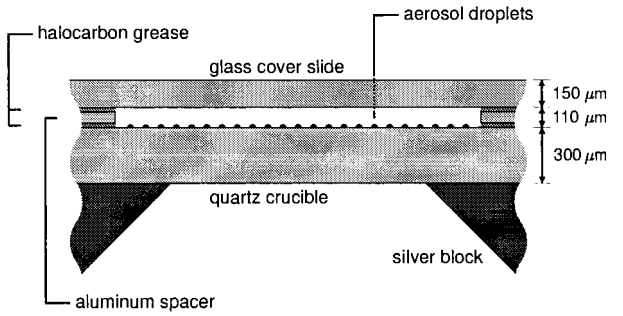

Figure 2. Sample cell.

stage. The microscope was used in transmitted light (brightfield) mode with two long-distance Zeiss objectives (magnification of 10× and 50×) and variable Optovar lenses (additional magnification of 1.25× and 1.6×). The cold stage substituted the regular microscope stage and the original top condenser lens was removed and replaced by a lens built into the silver block of the cold stage (see Figure 1). The aerosols could be observed via two focusing eyepieces (10x) and either a Video camera (Sony XC-75) connected to a videotape recorder and a monitor or a Zeiss photographic camera (MC-80). The BCS 196 cold stage is a closed system and can be sealed once the sample cell is located on a temperature-controlled silver block inside the cold stage. The sample cell can be moved in the $x-y$ plane by a crucible holder connected to two manipulators attached to the outside of the stage. Cooling is achieved by flowing cold N_2 gas from a liquid N_2 reservoir through the silver block, and the temperature was controlled by counterheating the silver block. Cooling and heating rates can be varied between 0.01 and 130 K min^{-1}. Both the interior and the upper window of the cold stage were purged with dry N_2 to avoid loss of optical resolution due to water condensation from room air during the experiments. The sample cell is shown in Figure 2. It consists of a quartz crucible (15 mm in diameter, 300 μm base thickness) and an aluminum washer about 60 μm thick with an inner diameter of about 2 mm. This setup can be closed by a glass cover slide 150 μm thick. The sealing between the crucible, the washer, and the slide was provided by two layers of Halocarbon grease about 25 μm thick. The total volume of the sample cell was about 3.5×10^{-4} cm^3. The quartz crucible base was treated prior to the experiments with a commercially available organosilane (Prosil 28), resulting in a monomolecular hydrophobic surface layer. This surface layer is water repellent and, thus, should minimize heterogeneous effects of the surface on the nucleation of hydrophilic ice. The aerosols were deposited onto the crucible with a nebulizer (Meinhard, TR-30). For a more detailed description of the nebulizer and the aerosol generation procedure, see Martin et al.[18] Briefly, H_2SO_4 aerosols were produced from a diluted H_2SO_4 solution by flowing N_2 through the nebulizer, and the aerosol stream was directed at the crucible for 1−2 s to deposit the aerosols. This led to an estimated particle coverage of about $1-3 \times 10^5$ cm^{-2}. The composition of the H_2SO_4 droplets could be changed by varying the total amount of water in the sample cell. The diameter of the deposited aerosols, as observed with the microscope, was between 5 and 20 μm depending on the H_2SO_4 concentration of the droplets (i.e., the upper limit being more representative for the experiments with the most dilute droplets and the lower limit representative for experiments with concentrated droplets). The contact angle of several larger droplets with the hydrophobic surface was measured using the microscope and observed to be between 50° and 70°. An average contact angle of 60° reduces the droplet volume by a factor of 4 when compared to a perfect sphere. Hence, the spherical equivalent diameter of the investigated droplets is smaller than the observed diameter by a factor of about 1.6, yielding spherical equivalent diameters between 3.1 and 12.6 μm for the droplets in the experiments reported below.

Temperature and Cooling-Rate Calibration. The temperature was measured with a resistance temperature sensor located in the upper part of the silver block as shown in Figure 1. The temperature calibration was performed in the range from 178.15 to 273.15 K by measuring the melting points of droplets and thin films of water (273.15 K), dodecane (263.55 K), octane (216.35 K), and toluene (178.15 K) in the sample cell. All freezing experiments were performed at a cooling rate of 10 K min^{-1}. Cooling rates smaller than about 2 K min^{-1} had the following unwanted effect: since nucleation is a stochastic process,[20] some droplets will always freeze earlier than others, even when maintained at the same temperature. The frozen aerosols have a smaller water vapor pressure than the remaining supercooled droplets, thus mass transport of water takes place leading to a growth of the frozen ice particles at the expense of the supercooled droplets. The volume of the liquid aerosols decreases accordingly, leading to an increase in H_2SO_4 concentration. In the extreme case (for infinitesimal cooling rates), the liquid droplets are in equilibrium with the few frozen ones at any temperature, implying that the remaining liquid droplets would never freeze since they are not supercooled, i.e., they are in equilibrium with ice. Experiments using varying cooling rates showed that a cooling rate of 10 K min^{-1} was fast enough to avoid this effect and the change in composition associated with it. On the other hand, large cooling rates led to an offset between the measured temperature in the silver block and the actual temperature at the quartz crucible surface where the droplets are located, because of heat-transfer limitations. Neglecting this experimental artifact would lead to lower observed freezing temperatures at larger cooling rates. To account for this artifact, we have performed freezing experiments with one sample of aerosols at varying cooling rates from 5 to 100 K min^{-1} as shown in Figure 3. The points correspond to the median freezing temperature of a number of H_2SO_4 droplets (2.1−2.4 wt %, Figure 3a) and octane droplets (Figure 3b). The freezing temperature stays almost constant for cooling rates smaller than about 20 K min^{-1} (0.05 min K^{-1}), while it significantly decreases for larger cooling rates. Hence, working

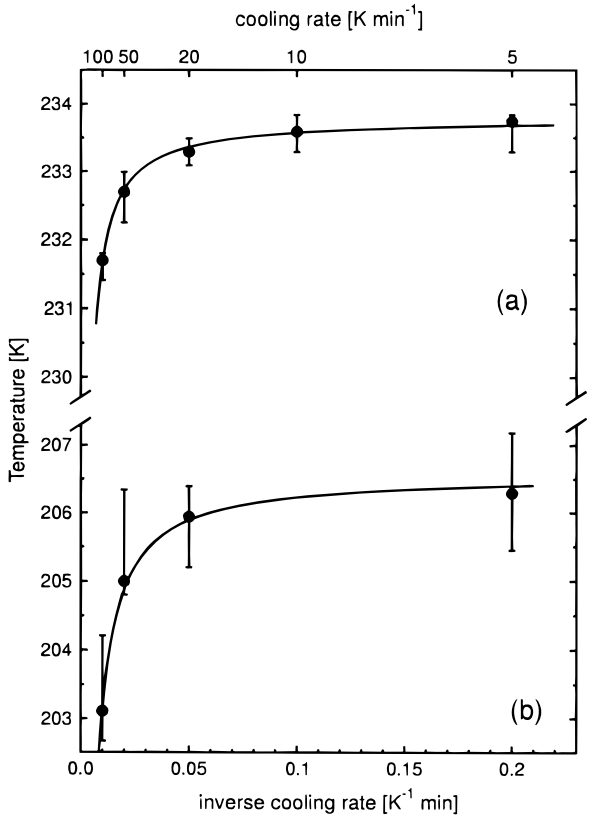

Figure 3. Median freezing temperature as a function of inverse cooling rate for (a) H_2SO_4 droplets 2.1−2.4 wt % in composition and (b) octane droplets. The error bars indicate the 20th and 80th percentiles, and the solid lines are least-squares fits to the data points.

at a cooling rate of 10 K min^{-1} (0.1 min K^{-1}) had only a small temperature bias and the corrections were between 0.2 K at 240 K and 0.5 K at 175 K.

Melting Points and Composition of Aerosols. The melting points of ice in the aqueous H_2SO_4 droplets were noted individually for each drop with an uncertainty of ±0.1 K. The melting point was then used to determine the composition of the droplet by using the thermodynamic model of Carslaw et al.[21] For each temperature, we calculated the water activity in solution for varying H_2SO_4 compositions until the water activity was equal to the one of ice at the same temperature. The melting-point curve calculated in this way is in excellent agreement with the original melting-point data by Gable et al.[22] However, to accurately determine the composition of the droplets from their melting points, one has to be sure that the composition of the droplets does not change with temperature. Since the equilibrium partial pressure of water over aqueous H_2SO_4 decreases with decreasing temperature, H_2SO_4 aerosols in the cell take up water with decreasing temperature to stay in equilibrium with the gas-phase water, thus reducing the water partial pressure in the cell. This water uptake would ordinarily dilute the H_2SO_4 droplets upon cooling. To avoid this change in composition, we used a large aerosol to gas-phase volume ratio by employing a small sample cell with a volume of 3.5 × 10^{-4} cm^3 (see Figure 2) and a large number of aerosol droplets with a total liquid volume of at least 4.9 × 10^{-8} cm^3. The dashed line of Figure 4 shows the calculated composition of aerosol droplets in the cell as a function of temperature for an initial composition of 24 wt % at 293 K. The solid line is the ice melting-point curve in aqueous H_2SO_4 solutions, implying that point M is the experimental ice melting point for this set of droplets. Furthermore, point F is the experimentally observed

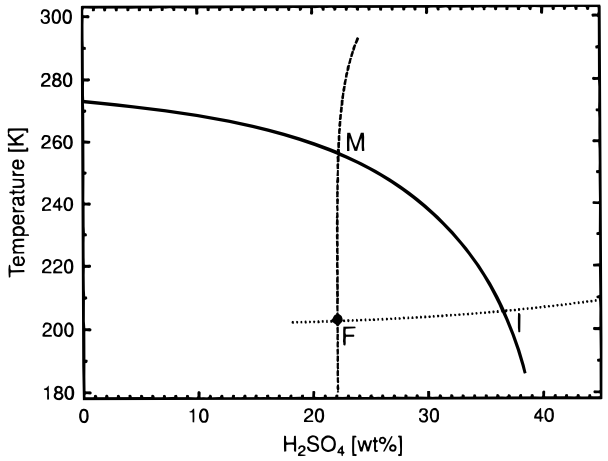

Figure 4. Compositions of aqueous H_2SO_4 aerosols as a function of temperature. Calculated H_2SO_4 aerosol composition trajectory for an experiment with an initial aerosol composition of 24 wt % at 293 K (- - -). Composition of atmospheric H_2SO_4 aerosols at an altitude of 200 mb (∼12 km) and a water mixing ratio of 20 ppmv (•••). Ice melting-point curve for the H_2SO_4/H_2O system (—). M: Melting point of ice for the H_2SO_4 aerosols following the experimental trajectory (- - -). F: Experimentally observed freezing temperature. I: Atmospheric ice frost point for the conditions along the atmospheric trajectory (•••). See text for more details.

freezing temperature (see below). Although there is an initial dilution of the droplets at higher temperatures, the composition curve becomes practically vertical below the melting point M. This is because the number of water molecules in the liquid is large compared to the number in the gas phase, so that the change in composition associated with the uptake of the appropriate amount of water between the melting point M and the freezing temperature F is only 0.15 wt % in this case. For all other compositions, this difference was calculated to be always less than 0.2 wt %. For comparison, we also show an atmospheric trajectory. The dotted line indicates the equilibrium composition of aqueous H_2SO_4 aerosols as a function of temperature for an altitude of 200 mb (∼12 km) and a H_2O mixing ratio of 20 ppmv. Upon cooling, the aerosols strongly dilute and become supercooled below point I, which is the atmospheric ice frost point under these conditions, until they finally freeze to form ice at point F. We also note that although the atmospheric composition trajectory is different from the experimental one, the freezing point F is the same in both cases.

Ice Nucleation Measurements. The H_2SO_4 droplets were cooled at a rate of 10 K min^{-1} to about 10−15 K below their observed freezing temperatures. Thereafter they were warmed to about 10 K below their melting points and then heated at a rate of 1 K min^{-1} until all particles were completely melted. The entire experiment was recorded on tape via the attached video system. Experimental conditions such as time, temperature, and magnification were converted into a video signal, overlayed on the camera signal, and recorded simultaneously. The tape was evaluated afterward to determine the freezing and melting points of individual droplets. In a typical experiment, a set of 20−70 droplets were monitored simultaneously. Each of them was marked on the video screen, and the melting and freezing temperature was determined individually for each drop to allow for small differences in concentration. This drop-by-drop evaluation turned out to be important in the concentration range of 25−27 wt %, where small differences in composition are associated with large changes in freezing temperature (see below). Figure 5 shows photographs of several aerosol droplets during the course of an experiment: Figure 5a shows aqueous

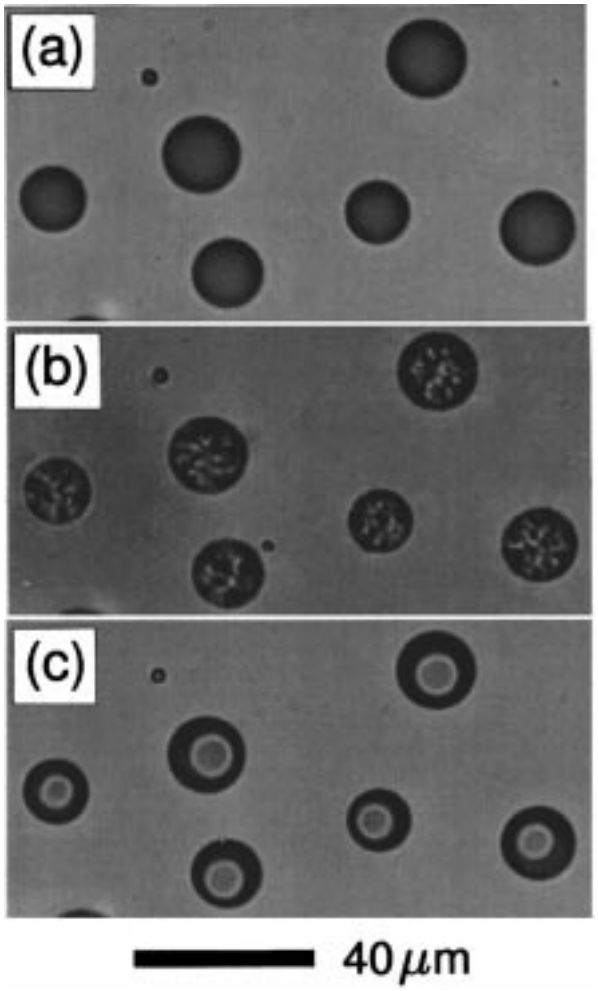

Figure 5. Photographs of a set of aqueous H_2SO_4 droplets during the course of an experiment. **(**a) Liquid droplets at 293 K. **(**b) Ice crystallized after cooling the droplets to 200 K. (c) Partially melted droplets at 266 K. The light circles within the droplets show the remaining ice.

H_2SO_4 aerosols (~11 wt %) in the liquid state at 293 K at the beginning of the experiment; Figure 5b shows that ice has crystallized after cooling the droplets to 200 K; while Figure 5c shows that the ice is melting again when heated to 266 K.

Results and Discussion

A total number of 1214 H_2SO_4 aerosol droplets have been examined, and their ice freezing temperatures are shown as a function of composition in Figure 6. Although there is scatter owing to the stochastic nature of the nucleation process, the collected freezing temperatures fall on a well-defined curve. It is interesting to note that the supercooling with respect to the melting point as a function of composition is not constant but increases strongly at higher concentration to a value of about 66 K at 26 wt %. These raw data points were subsequently evaluated in the following way: All droplets were sorted into bins according to their composition, with a bin width of 0.2 wt %. Then the median of the freezing temperatures of all droplets in each bin was calculated for all bins containing at least 6 data points. We choose to calculate the median rather than the average freezing temperature because the freezing temperatures are not normally distributed around the temperature where the maximum number of freezing events occur (see also Pruppacher and Klett[23]). Also, a few droplets freezing heterogeneously at

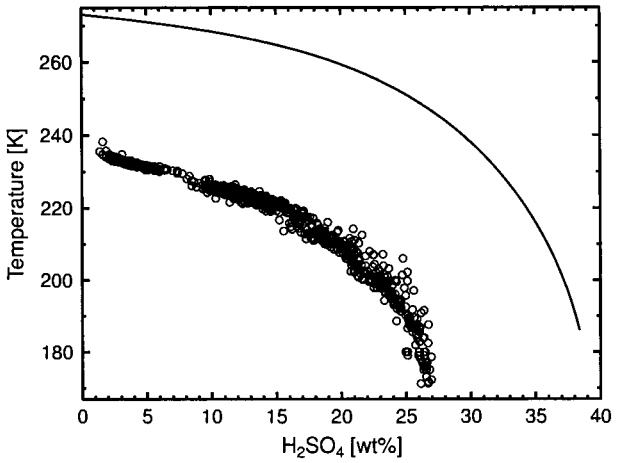

Figure 6. Measured ice freezing temperatures for a total of 1214 H_2SO_4 droplets. Each circle represents the freezing temperature of a single aerosol. The line indicates the ice melting-point curve.

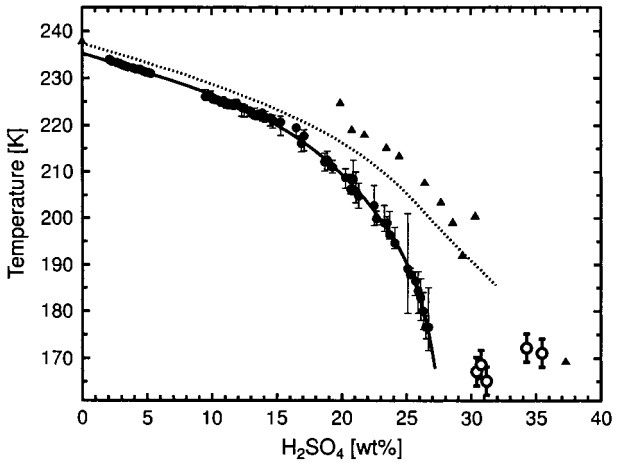

Figure 7. Comparison between different H_2SO_4 aerosol freezing temperature data sets. Median freezing temperatures (●), this work. The error bars indicate the 20th and 80th percentiles, and the solid line is a least-squares fit to the data points (see Table 1). Freezing temperatures obtained by Bertram et al. (▲).[12] Freezing temperature parametrization of Tabazadeh et al.[29] based on the data of Bertram et al. (- - -).[12] Temperature where a droplet with an effective diameter of 135 μm crystallized upon warming (no freezing was observed upon cooling to 140 K) (○). The error bars represent the temperature uncertainty.

TABLE 1: Critical Ice Nucleation Temperature as a Function of H_2SO_4 Concentration[a]

	A_0	A_1	A_2	A_3
T^*	235.28	−0.81592	$-5.8949\cdot10^{-5}$	$-2.0021\cdot10^{-11}$

[a] T^* can be calculated from $T^* = A_0 + A_1(wt) + A_2(wt)^4 + A_3 \exp(wt)$, where T^* is the critical ice nucleation temperature [in K] and wt is the H_2SO_4 concentration [in wt %]. This relation is valid from 0 to 26.5 wt %.

higher temperatures have a much smaller impact on the median freezing temperature than on the average. The evaluated data is shown as full circles in Figure 7; the error bars represent the 20th and 80th percentiles. The solid line is a least-squares fit to the median freezing temperatures, and the parameters describing the curve are given in Table 1. For comparison, we also show as triangles the ice freezing temperatures of Bertram et al.[12] which were obtained in flow-tube aerosol experiments. These experiments were performed by continuously producing H_2SO_4 aerosols about 0.4 μm in diameter in a flow tube and controlling their composition by changing the water partial

pressure in the gas stream. The flow-tube temperature was varied, and composition and freezing was detected by means of FTIR spectroscopy, i.e., by observing characteristic liquid H_2SO_4 and ice absorption features in the spectra. The freezing temperatures of Bertram et al.[12] are systematically higher than our measurements, in particular for concentrations larger than about 20 wt %. The highest concentration for which we observed freezing is 26.7 wt %, while Bertram et al.[12] still observe freezing at 37.3 wt %, revealing a difference in H_2SO_4 concentration of more than 10 wt %. The higher freezing temperatures in Bertram et al.[12] are surprising, particularly because their aerosol droplets were smaller than ours, which should have lower rather than higher freezing temperatures since the nucleation probability is proportional to the liquid aerosol volume. To ensure that in fact no ice freezing occurs in aerosols more concentrated than about 27 wt %, we performed several experiments with a large H_2SO_4 droplet, about 215 μm in diameter (spherical equivalent diameter about 135 μm), and with a composition ranging from 30.4 to 35.4 wt %. This droplet did not freeze upon cooling in five out of six experiments when cooled at a rate of 10 K min^{-1} to 140 K, and crystallization occurred only upon warming to temperatures of about 165−172 K (open circles in Figure 7). In contrast to our observations, the 0.4 μm droplet freezing data of Bertram et al.[12] imply that such big particles would freeze well above 170 K. The differences between our study and the one of Bertram et al.[12] cannot be explained by the stochastic nature of the nucleation process, since the variation in freezing temperatures in our experiments are smaller than the discrepancies between the different experiments. We can only speculate that the exact determination of the H_2SO_4 concentration of the aerosols in Bertram et al.[12] might be the reason; note also that infrared absorption spectra for liquid H_2SO_4/H_2O solutions in this concentration range are not available at low temperatures and had to be extrapolated from higher-temperature measurements. These authors estimate an uncertainty in their H_2SO_4 concentration of ±7 wt %, which is about as big as the difference of 10 wt % between our data and their data. Clapp et al.[14] also observed the freezing of ice from H_2SO_4 aerosols 25−38 wt % in composition above 170 K. However, since they were using an experimental technique very similar to the one of Bertram et al.,[12] the differences between their data and our data can be explained by the same reasons. MacKenzie et al.[24] have performed a theoretical study on the nucleation of ice from binary H_2SO_4/H_2O solutions using a simplification of the classical nucleation equation. They calculated significantly higher ice freezing temperatures than those observed in our experiments for solutions between 15 and 35 wt %, implying that their approach works better at more dilute solutions. The freezing upon warming points reported here (open circles in Figure 7) also reveal another piece of important information. Freezing involves two processes: nucleation of a stable germ and crystal growth of this germ to freeze the whole liquid droplet (see Koop et al.[20] for a more detailed discussion on this matter). However, at temperatures below about 170 K, the viscosity of aqueous H_2SO_4 becomes so large that the crystal growth of ice is only very slow. Hence, the droplets do not freeze even if germs have nucleated. On the other hand, at higher temperatures, the crystal growth is fast enough that the droplets freeze practically instantaneous once a germ nucleates. This was also observed when evaluating the video in slow motion, showing the ice crystals growing within a fraction of a second at the higher temperatures (235−200 K) but requiring up to about 1 s at 170 K for a 20 μm droplet to freeze completely.

Heterogeneous Effects. Did the surface supporting the droplets during the experiments have any effect on the freezing temperature, i.e., did heterogeneous nucleation take place in our experiments? Although heterogeneous nucleation can never be excluded with absolute certainty, we have some strong arguments suggesting it was unimportant in the experiments described above. First, as pointed out earlier, our freezing temperatures are lower than the ones obtained in experiments with unsupported droplets, thus suggesting that our data are much closer to the real homogeneous freezing temperature than the older data set. Second, a few out of the total of 1214 droplets evaluated in this study froze at significantly higher temperatures than the rest of the ensemble, which can be seen, for example, in Figure 6. One of the most dilute droplets and several droplets at concentrations between 20 and 25 wt % froze a few Kelvin above the main portion of the droplets. We think these freezing temperatures were influenced by heterogeneous freezing due to either defects in the hydrophobic surface coating or a dust particle enclosed in the droplets. However, since we took the median freezing temperature, none of these points had a significant effect on the freezing results reported above. Finally, we compared our freezing temperature for infinite dilution, i.e., for pure water, with the homogeneous freezing point for water reported in the literature. Recently, Pruppacher[25] evaluated all the available data on the homogeneous nucleation of ice from pure water and fitted the data to an empirical function for the temperature dependence of the homogeneous nucleation rate constant, $J(T)$. Using this function $J(T)$, the median freezing temperature for homogeneous ice nucleation from an ensemble of water droplets can be calculated from[23]

$$\int_{T_m}^{T_0} J(T)\mathrm{d}T = 0.693\gamma_c/V_d \qquad (1)$$

where T_m is the median freezing temperature, T_0 is a temperature where all droplets are still liquid (chosen to be at 240.15 K in our case, at which $J(T)$ contributes only negligibly), $J(T)$ is the homogeneous nucleation rate constant (see above), γ_c is the cooling rate, and V_d is the individual droplet volume. For our experimental cooling rate of 10 K min^{-1} and our spherical equivalent droplet diameters, the calculated T_m for homogeneous water freezing would be between 235 and 236 K for our experimental conditions. The experimentally determined T_m for pure water with our microscope technique is 235.3 K (see Table 1), which is in excellent agreement with the calculated homogeneous freezing temperature. We consider this to be a strong argument in showing that the ice nucleation in our experiment was not influenced by the supporting surface but was indeed homogeneous.

Atmospheric Implications. Cirrus clouds and ice PSCs are believed to form from sulfate aerosols, which are ubiquitous in the upper troposphere and lower stratosphere. However, in situ measurements of the formation conditions of these clouds are difficult. Detailed field measurements together with microphysical modeling have become available only very recently from orographically induced wave clouds on the cirrus level[26,27] and in the lower stratosphere.[28] In the following sections, we describe some thermodynamic calculations we performed in order to relate the experimental results presented above to the atmosphere, thus allowing a comparison between laboratory data and field observations.

Thermodynamic Modeling. Recently, Tabazadeh et al.[29] used the data of Bertram et al.[12] to constrain a model describing the homogeneous nucleation kinetics of ice from H_2SO_4/H_2O solutions. The model was then applied to the formation of cirrus

TABLE 2: Critical Ice Nucleation Parameters, *X, as a Function of the Atmospheric Water Partial Pressure P_{H_2O}[a]**

X^*	A_0	A_1	A_2	A_3	A_4	A_5
T^*	$2.534379\cdot10^{+2}$	$1.577798\cdot10^{+1}$	$3.063374\cdot10^{+0}$	$6.160317\cdot10^{-1}$	$6.464393\cdot10^{-2}$	$2.602547\cdot10^{-3}$
wt^*	$-2.872851\cdot10^{+1}$	$-2.715777\cdot10^{+1}$	$-6.116733\cdot10^{+0}$	$-7.078192\cdot10^{-1}$	$-3.742763\cdot10^{-2}$	$-5.913863\cdot10^{-4}$
a_w^*	$1.065212\cdot10^{+0}$	$4.419819\cdot10^{-2}$	$-8.428876\cdot10^{-4}$	$-3.034403\cdot10^{-4}$	$7.187931\cdot10^{-7}$	$8.797225\cdot10^{-7}$
S_{ice}^*	$1.307397\cdot10^{+0}$	$-1.233811\cdot10^{-1}$	$-2.780350\cdot10^{-2}$	$-4.762990\cdot10^{-3}$	$-4.587159\cdot10^{-4}$	$-1.788353\cdot10^{-5}$
ΔT^*	$-2.915564\cdot10^{+0}$	$4.700823\cdot10^{-1}$	$1.512852\cdot10^{-1}$	$2.089472\cdot10^{-2}$	$1.542953\cdot10^{-3}$	$4.789159\cdot10^{-5}$

[a] The different critical ice nucleation parameters, X^*, can be calculated from $X^* = \sum_{i=0}^{5} A_i(\ln P_{H_2O})^i$, where P_{H_2O} is the atmospheric water partial pressure [in mb], T^* is the critical temperature [in K], wt^* is the critical composition [in wt %], a_w^* is the critical water activity (which is equal to the critical relative humidity), S_{ice}^* is the critical ice saturation ratio, and ΔT^* is the critical cooling below the ice frost point [in K]. These parametrizations are valid over the water partial pressure range from 2.3×10^{-1} to 2.2×10^{-4} mb. For verification, at $P_{H_2O} = 10^{-2}$ mb, the above parameters yield the follwing values for the different X^*: $T^* = 209.26$, $wt^* = 20.14$, $a_w^* = 0.8719$, $S_{ice}^* = 1.582$, and $\Delta T^* = -3.318$.

clouds to predict the conditions under which ice particles would nucleate from H_2SO_4 aerosols in the upper troposphere. Here we show how incorporating the new ice freezing temperature data shown in Figure 7 affects the critical parameters for the formation of ice particles from H_2SO_4 aerosols. We follow the same approach as Tabazadeh et al.,[29] using, however, our new ice freezing data to constrain the model. The water saturation vapor pressure and the ice saturation vapor pressure were taken directly from Tabazadeh et al.,[29] and the water activity in the liquid phase was calculated from the model of Carslaw et al.,[21] which is the same as the binary H_2SO_4/H_2O model of Clegg and Brimblecombe[30] used by Tabazadeh et al.[29] This was done to ensure that the difference in the new parametrization is solely due to the different experimental data while keeping consistency between the calculations by using identical thermodynamic models. The critical H_2SO_4 concentration and the critical temperature for ice nucleation given in Table 1 were used as the experimental input data. The critical water activity, a_w^*, and the water vapor pressure, P_{H_2O}, were calculated directly from the model. The critical ice saturation ratio, S_{ice}^*, was calculated as

$$S_{ice}^* = \frac{P_{H_2O}^*(T^*, wt^*)}{P_{ice}(T^*)} \tag{2}$$

where $P_{H_2O}^*(T^*, wt^*)$ is the equilibrium water partial pressure of an H_2SO_4/H_2O aerosol at the critical temperature T^* and the critical composition wt^* and $P_{ice}(T^*)$ is the water vapor pressure of ice at T^*. Finally, the critical cooling below the ice frost point, ΔT^*, was calculated from

$$\Delta T^* = T_{ice}(P_{H_2O}^*) - T^* \tag{3}$$

where $T_{ice}(P_{H_2O}^*)$ is the atmospheric ice frost point temperature for the critical water partial pressure P_{H_2O} at T^*. All the parameters were fitted as a function of the water partial pressure to allow easier comparison to field measurements. The different critical parameters for ice nucleation from H_2SO_4 aerosols are given in Table 2. We note again that the differences between this parametrization and the formulas given by Tabazadeh et al.[29] are solely due to the different experimental data used to constrain the model while the models themselves are identical. This means that the different thermodynamic models describing the water activity in H_2SO_4 solutions at low temperatures can be used interchangeably with this new parametrization. The two most important parameters in terms of cloud modeling and observations are probably the critical saturation ratio with respect to ice, S_{ice}^*, or equivalently the critical cooling below the ice frost point, ΔT^*, needed to form the ice particles. Both are shown as a function of temperature in Figures 8 and 9, respectively. The solid lines indicate our new parametrization, and the dashed lines indicate the one by Tabazadeh et al.[29] based on the data of Bertram et al.[12] The old parametrization shows a maximum value for S_{ice}^* of about 1.51 at 213 K, sharply decreasing to about 1.35 at 186 K (see Figure 8). Our new data shows instead that S_{ice}^* continues to increase with decreasing temperatures, its values ranging from 1.57 at 213 K to 1.67 at 185 K. Also, on the basis of the old parametrization, the critical cooling below the ice frost point ΔT^* is about -3.3 K at temperatures around 230 K and then rises to approximately -1.7 K at 186 K (see Figure 9). In contrast, our new values start at -3.4 K for $T \geq 230$ K, with only a small increase to

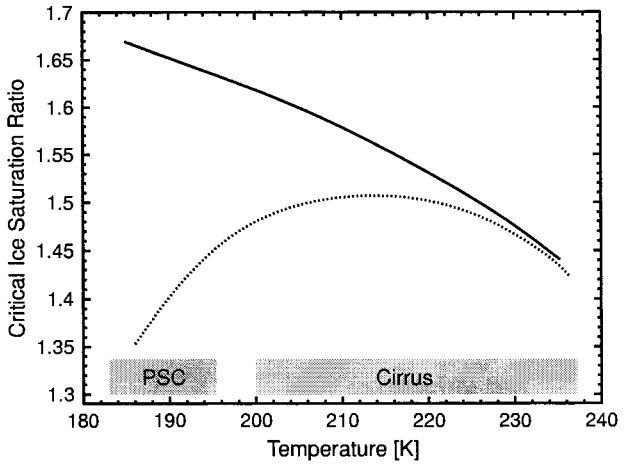

Figure 8. Critical ice saturation ratio, S_{ice}^*, as a function of temperature: this work (—); parametrization of Tabazadeh et al.[29] based on the data of Bertram et al. (•••).[12] The gray areas indicate the temperature regimes where PSCs and cirrus clouds are most commonly observed.

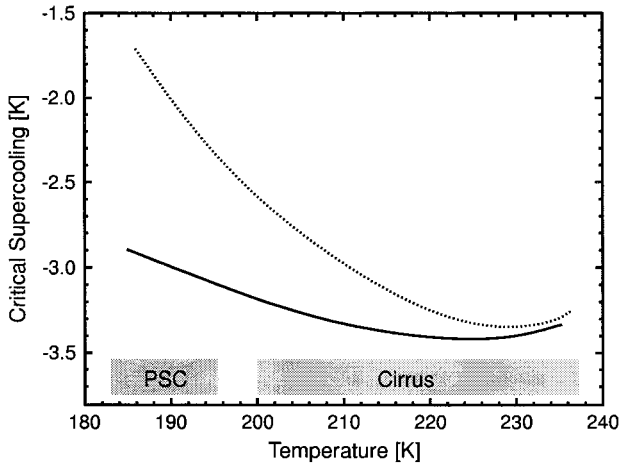

Figure 9. Critical cooling below the ice frost point, ΔT^*, as a function of temperature: this work (—); parametrization of Tabazadeh et al.[29] based on the data of Bertram et al. (•••)[12] The gray areas indicate the temperature regimes where PSCs and cirrus clouds are most commonly observed.

−2.9 K at 185 K. This has important consequences for our understanding of the formation of both cirrus clouds and PSCs.

Cirrus Clouds. Sulfate aerosols are thought to be involved in the formation of cirrus clouds in the upper troposphere, and under clean conditions, these sulfate aerosols are believed to be composed of binary H_2SO_4/H_2O solutions.[2,31−33] During the recent field experiment SUCCESS (Subsonic Aircraft: Contrail and Cloud Effects Special Study[7]), high supersaturations in tropospheric clouds were observed.[26] The in situ measurements near the leading edge of a wave cloud at 209 K revealed a maximum saturation ratio with respect to ice of about 1.6.[26,27] Jensen et al.[27] compared these measurements to numerical simulations for the formation of ice from H_2SO_4/H_2O aerosols using the parametrization of Tabazadeh et al.;[29] they calculated a maximum saturation ratio of 1.5, which is much closer to the in situ measurements than an earlier value of about 1.3 calculated by these authors using a different parametrization.[34] In contrast, using the parametrization based on our new laboratory data, we obtain a value of about 1.6, in excellent agreement with the measured value. In a sensitivity study, Jensen et al.[27] increased the critical saturation ratio to 1.6 (no. 9 in their Table 2), leading to a calculated peak ice particle number concentration of 5.7 cm^{-3}, which falls within the observed range of 2−7 cm^{-3}. These comparisons indicate that our new parametrization yields the best agreement between observations and microphysical simulations in the case of orographic wave clouds. In the case of wave clouds where strong cooling occurs due to high updraft velocities, heterogeneous nuclei probably play only a minor role. If only a few ice particles form heterogeneously, they would need time to grow to remove the available water vapor from the surrounding air, thus decreasing the supersaturation. However, in wave clouds, the supersaturation rises so quickly due to the large updraft velocities that these few ice particles do not have time to remove a significant amount of water vapor before a supersaturation is reached, at which the majority of the remaining liquid aerosols freeze homogeneously, leading to a sharp decrease in the relative humidity. On the other hand, in the case of slow gradual cooling, heterogeneous nucleation will have a much stronger impact because a few heterogeneously nucleated ice particles have time to grow and remove the water vapor from the gas phase and, hence, decrease the supersaturation.[35] The supersaturation needed to induce homogeneous ice nucleation from binary H_2SO_4/H_2O revealed in this paper is higher than that previously thought and, thus, increases the chance for heterogeneous nuclei to play a more important role. Further studies will be needed to investigate both the effect of heterogeneous nuclei[35] and also the incorporation of NH_3 and HNO_3 into the aerosols[36,37] on the formation conditions of ice cirrus clouds.

Polar Stratospheric Clouds. Previously, it was generally believed that ice would freeze without much supercooling from stratospheric aerosols and usually a critical cooling of about 1 K below the ice frost point was assumed.[34,38] On the basis of the H_2SO_4/H_2O data by Bertram et al.,[12] Tabazadeh et al.[29] suggested that a value of about 1.7−2 K would be more appropriate at stratospheric temperatures. For binary HNO_3/H_2O aerosols, they calculated values of about 2.0−2.5 K at stratospheric temperatures.[39] On the other hand, Carslaw et al.[28] inferred a cooling of 3−4 K in ternary $HNO_3/H_2SO_4/H_2O$ aerosols from in situ lidar measurements of a stratospheric lee wave ice cloud. Our new data set suggests that binary H_2SO_4/H_2O aerosols freeze about 3 K below the ice frost point at stratospheric temperatures, which is more than 1 K lower than the value calculated by Tabazadeh et al.[29] This difference of 1 K does not seem to be very much. However, at the same time, the ice saturation ratio, which is the key factor in the microphysics of ice formation, changes from 1.35 to 1.65, hence producing ice clouds with very different size distributions and ice particle number densities. This has important consequences for the lifetime and the optical properties of these clouds. Although our value of 3 K cooling below the ice frost point is very close to the observation by Carslaw et al.,[28] ice nucleation in the stratosphere seldom occurs from binary H_2SO_4/H_2O aerosols, because H_2SO_4 is the main aerosol component at low temperatures only under volcanically perturbed conditions. However, under volcanically quiet conditions, HNO_3 uptake will occur in stratospheric aerosols several degrees above the frost point, so that ice nucleates from either ternary $HNO_3/H_2SO_4/H_2O$ or nearly binary HNO_3/H_2O aerosols. The calculations of Tabazadeh et al.[39] suggest that binary HNO_3/H_2O aerosols would require a larger cooling than binary H_2SO_4/H_2O aerosols, but recent laboratory measurements suggest a similar cooling of about 3 K.[40] In the case of high sulfate loading, we suggest that a cooling of about 3 K would be required to form ice from stratospheric aerosols.

Conclusions

In this paper, we have presented a new technique to study liquid−solid phase transitions in aerosol particles. This optical microscope technique allows us to obtain information on the phase-transition temperatures and also on the composition of the aerosols under investigation, which is more direct than has been achieved in the past with flow-tube or settling-chamber studies coupled to FTIR spectroscopy. We have used the microscope technique to investigate the temperatures at which ice nucleates from H_2SO_4/H_2O aerosols with concentrations in the range from 0 to 35 wt %. The experiments reveal that a supercooling of up to 66 K is needed to form the ice, much higher than was inferred from earlier calculations and measurements. A thermodynamic model has been used to apply the new freezing temperature data to the formation of clouds in the upper troposphere and lower stratosphere. The results indicate that the homogeneous nucleation of ice in cirrus clouds requires saturation ratios with respect to ice of up to 1.6, in excellent agreement with in situ observations of tropospheric wave clouds published recently. The cooling below the frost point for the formation of ice PSCs is predicted to be about 3 K, which is also in much closer agreement with recent field observations than the previously published value.

Acknowledgment. We thank A. Chang for his help with the preliminary development of this technique, A. Bertram for providing us with his freezing temperature data, and A. Tabazadeh for sending us her H_2SO_4 ice nucleation code. This work was supported by grants from NASA's Atmospheric Effects of Aviation Program, the National Science Foundation, and the Max Planck Research Award to M. Molina and P. Crutzen. T.K. gratefully acknowledges a Feodor Lynen Fellowship from the Humboldt Foundation and an Otto Hahn Fellowship from the Max Planck Society.

References and Notes

(1) *Intergovernmental Panel on Climate Change (IPCC), Climate Change 1995*; Houghton, J. T., Meira Filho, L. G., Callander, B. A., Harris, N., Kattenberg, A., Marshall, K., Eds.; Cambridge University Press: Cambridge, 1996.

(2) Seinfeld, J. H. *Nature* **1998**, *391*, 837.

(3) Liou, K. N. *Mon. Weather Rev.* **1986**, *114*, 1167.

(4) Borrmann, S.; Solomon, S.; Dye, J. E.; Luo, B. P. *Geophys. Res. Lett.* **1996**, *23*, 2133.
(5) Reichardt, J.; Ansmann, A.; Serwazi, M.; Weitkamp, C.; Michaelis, W. *Geophys. Res. Lett.* **1996**, *23*, 1929.
(6) Kley, D.; Crutzen, P. J.; Smit, H. G. J.; Vömel, H.; Oltmans, S. J.; Grassl, H.; Ramanathan, V. *Science* **1996**, *274*, 230.
(7) Toon, O. B.; Miake-Lye, R. C. *Geophys. Res. Lett.* **1998**, *25*, 1109.
(8) World Meteorological Organization, Scientific assessment of ozone depletion: 1994, Report No. 37, Geneva, 1995.
(9) Koop, T.; Carslaw, K. S.; Peter, T. *Geophys. Res. Lett.* **1997**, *24*, 2199.
(10) Shindell, D. T.; Rind, D.; Lonergan, P. *Nature* **1998**, *392*, 589.
(11) Anthony, S. E.; Tisdale, R. T.; Disselkamp, R.; Tolbert, M. A.; Wilson, J. C. *Geophys. Res. Lett.* **1995**, *22*, 1105.
(12) Bertram, A. K.; Patterson, D. D.; Sloan, J. J. *J. Phys. Chem.* **1996**, *100*, 2376.
(13) Disselkamp, R.; Anthony, S. E.; Prenni, A. J.; Onasch, T. B.; Tolbert, M. A. *J. Phys. Chem.* **1996**, *100*, 9127.
(14) Clapp, M. L.; Niedziela, R. F.; Richwine, L. J.; Dransfield, T.; Miller, R. E.; Worsnop, D. R. *J. Geophys. Res.* **1997**, *102*, 8899.
(15) Bertram, A. K.; Sloan, J. J. *J. Geophys. Res*. **1998**, *103*, 3553.
(16) Molina, M. J.; Chang, H. Y. A.; Martin, S. T.; Molina, L. T.; Ng, H. P.; Salcedo, D. Paper presented at the 1997 Conference on the Atmospheric Effects of Aviation, March 10−14, Virginia Beach, VA, 1997.
(17) Chang, H. Y. A. Experimental Studies of the Formation Mechansims of Type I Polar Stratospheric Clouds, Ph.D. Thesis, Massachusetts Institute of Technology, Cambridge, MA, 1996.
(18) Martin, S. T.; Salcedo, D.; Molina, L. T.; Molina, M. J. *J. Phys. Chem. B* **1997**, *101*, 5307.
(19) Ng, H. P. Investigation of Freezing Properties of Polar Stratospheric Cloud Particles with Optical Microscopy, M.S. Thesis, Massachusetts Institute of Technology, Cambridge, MA, 1997.
(20) Koop, T.; Luo, B. P.; Biermann, U. M.; Crutzen, P. J.; Peter, T. *J. Phys. Chem. A* **1997**, *101*, 1117.
(21) Carslaw, K. S.; Clegg, S. L.; Brimblecombe, P. *J. Phys. Chem.* **1995**, *99*, 11557.
(22) Gable, C. M.; Betz, H. F.; Maron, S. H. *J. Am. Chem. Soc.* **1950**, *72*, 1445.
(23) Pruppacher, H. R.; Klett, J. D. Microphysics of Clouds and Precipitation, 2nd ed.; Kluwer: Dordrecht, 1997.
(24) MacKenzie, A. R.; Laaksonen, A.; Batris, E.; Kulmala, M. *J. Geophys. Res.* **1998**, *103*, 10875.
(25) Pruppacher, H. R. *J. Atmos. Sci.* **1995**, *52*, 1924.
(26) Heymsfield, A. J.; Miloshevich, L. M.; Twohy, C.; Sachse, G.; Oltmans, S. *Geophys. Res. Lett.* **1998**, *25*, 1343.
(27) Jensen, E. J.; Toon, O. B.; Tabazadeh, A.; Sachse, G. W.; Anderson, B. E.; Chan, K. R.; Twohy, C. W.; Gandrud, B.; Aulenbach, S. M.; Heymsfield, A.; Hallett, J.; Gary, B. *Geophys. Res. Lett.* **1998**, *25*, 1363.
(28) Carslaw, K. S.; Wirth, M.; Tsias, A.; Luo, B. P.; Dörnbrack, A.; Leutbecher, M.; Volkert, H.; Renger, W.; Bacmeister, J. T.; Peter, T. *J. Geophys. Res.* **1998**, *103*, 5785.
(29) Tabazadeh, A.; Jensen, E. J.; Toon, O. B. *J. Geophys. Res*. **1997**, *102*, 23845.
(30) Clegg, S. L.; Brimblecombe, P. *J. Chem. Eng. Data* **1995**, *40*, 43.
(31) Sassen, K.; Dodd, G. C. *J. Atmos. Sci.* **1989**, *46*, 3005.
(32) Heymsfield, A. J.; Sabin, R. M. *J. Atmos. Sci.* **1989**, *46*, 2252.
(33) Jensen, E. J.; Toon, O. B.; Westphal, D. L.; Kinne, S.; Heymsfield, A. J. *J. Geophys. Res.* **1994**, *99*, 10421.
(34) Jensen, E. J.; Toon, O. B.; Hamill, P. *Geophys. Res. Lett.* **1991**, *18*, 1857.
(35) DeMott, P. J.; Rogers, D. C.; Kreidenweis, S. M.; Chen, Y. L.; Twohy, C. H.; Baumgardner, D.; Heymsfield, A. J.; Chan, K. R. *Geophys. Res. Lett.* **1998**, *25*, 1387.
(36) Laaksonen, A.; Hienola, J.; Kulmala, M.; Arnold, F. *Geophys. Res. Lett.* **1997**, *24*, 3009.
(37) Tabazadeh, A.; Toon, O. B. *Geophys. Res. Lett.* **1998**, *25*, 1379.
(38) Koop, T.; Biermann, U. M.; Raber, W.; Luo, B. P.; Crutzen, P. J.; Peter, T. *Geophys. Res. Lett.* **1995**, *22*, 917.
(39) Tabazadeh, A.; Toon, O. B.; Jensen, E. J. *Geophys. Res. Lett.* **1997**, *24*, 2007.
(40) Chang, H. Y. A.; Koop, T.; Molina, L. T.; Molina, M. J. *J. Phys. Chem.*, submitted for publication.